

The variability behavior of CoRoT M-giant Stars [★]

C. E. Ferreira Lopes^{1,2}, V. Neves¹, I. C. Leão¹, D. B. de Freitas¹, B. L. Canto Martins¹, A. D. da Costa¹, F. Paz-Chinchón¹, M. L. Das Chagas¹, A. Baglin³, E. Janot-Pacheco⁴, and J. R. De Medeiros¹

¹ Departamento de Física, Universidade Federal do Rio Grande do Norte, Natal, RN, 59072-970 Brazil
e-mail: carlos_eduardo@dfte.ufrn.br

² SUPA (Scottish Universities Physics Alliance) Wide-Field Astronomy Unit, Institute for Astronomy, School of Physics and Astronomy, University of Edinburgh, Royal Observatory, Blackford Hill, Edinburgh EH9 3HJ, UK

³ LESIA, UMR 8109 CNRS, Observatoire de Paris, UVSQ, Université Paris-Diderot, 5 place J. Janssen, 92195 Meudon, France

⁴ Universidade de São Paulo/IAG-USP, rua do Matão, 1226, Cidade Universitária, São Paulo, SP, 05508-900 Brazil

Received Month Day, Year; accepted Month Day, Year

ABSTRACT

Context. For 6 years the Convection, Rotation, and Planetary Transits (CoRoT) space mission has acquired photometric data from more than one hundred thousand point sources towards and directly opposite from the inner and outer regions of the Galaxy. The high temporal resolution of the CoRoT data combined with the wide timespan of the observations has enabled the study of short and long time variations in unprecedented detail.

Aims. The aim of this work is the study of the variability and evolutionary behavior of M-giant stars using CoRoT data.

Methods. From the initial sample of 2534 stars classified as M-giants in the CoRoT databasis, we selected 1428 targets that exhibit well defined variability, using visual inspection. Then, we defined three catalogs: C1 – stars with $T_{\text{eff}} < 4200$ K and LCs displaying semi-sinusoidal signatures; C2 – rotating variable candidates with $T_{\text{eff}} > 4200$ K; C3 – long period variable candidates (with LCs showing variability period up to the total time span of the observations). The variability period and amplitude of C1 stars were computed using Lomb-Scargle and harmonic fit methods. Finally, we used C1 and C3 stars to study the variability behavior of M-giant stars.

Results. The trends found in the $V - I$ vs $J - K$ color-color diagram are in agreement with standard empirical calibrations for M-giants. The sources located towards the inner regions of the Galaxy are distributed throughout the diagram while the majority of the stars towards the outer regions of the Galaxy are spread between the calibrations of M-giants and the predicted position for Carbon stars. The stars classified as supergiants follow a different sequence from the one found for giant stars. We also performed a KS test of the period and amplitude of stars towards the inner and outer regions of the Galaxy. We obtained a low probability that the two samples come from the same parent distribution. The observed behavior of the period-amplitude and period-effective temperature (T_{eff}) diagrams are, in general, in agreement with those found for *Kepler* sources and ground based photometry, with pulsation being the dominant cause responsible for the observed modulation. We also conclude that short-time variations on M-Giant stars do not exist or are very rare and the few cases we found are possibly related to biases or background stars.

Key words. Astronomical data bases: Catalogs – Stars: Oscillation (including pulsation) – Stars: Evolution.

1. Introduction

The Convection, Rotation, and Planetary Transits (CoRoT; Baglin et al. 2007) and *Kepler* (Borucki et al. 2010) photometry space missions, have enabled us to improve our knowledge of a large variety of stellar phenomena, such as the rotational behavior of different families of stars (e.g., Affer et al. 2012; De Medeiros et al. 2013; Nielsen et al. 2013; McQuillan et al. 2013; de Freitas et al. 2013), detection and characterization of a wide variety of extrasolar planets (e.g., Léger et al. 2009; Borucki et al. 2012; Batalha et al. 2013) and their host stars (e.g., Brown et al. 2011; Dressing & Charbonneau 2013; Morton & Swift 2014; Huber et al. 2014), the analysis of stellar interiors using asteroseismology (e.g., Huber et al. 2012; Silva Aguirre et al. 2012; Hekker et al. 2013); characterization of surface differential rotation (Lanza et al. 2014); and the detection of eclipsing binary systems (e.g., Maceroni et al. 2009;

Slawson et al. 2011; Maciel et al. 2011). The aforementioned science cases are only a few major topics among the many aspects of time-domain, high-precision photometry. The data provided by the CoRoT and *Kepler* space missions represent the most complete dataset for the study of stellar variability available to date (e.g., De Medeiros et al. 2013; Walkowicz & Basri 2013). In general the results from each mission agree with each other, but there is a lack of a comparative study regarding M-type stars.

One of the fundamental questions in debate in the literature is the evolution and nature of the pulsations in M giants. Our recent understanding of how M giants oscillate was obtained from ground-based surveys such as MACHO, OGLE, and EROS (e.g. Wood & Sebo 1996; Alard et al. 2001; Lebzelter et al. 2002; Kiss & Bedding 2003; Soszynski et al. 2007; Riebel et al. 2010; Wiśniewski et al. 2011; Soszynski et al. 2013), as well as solar neighbourhood observations (Tabur et al. 2010).

Another important question concerns the evolution and nature of the pulsations in the GK-M type giant transition in the RGB. Whether the main physical mechanism of the pulsations

[★] The CoRoT space mission was developed and is operated by the French space agency CNES, with the participation of ESA's RSSD and Science Programmes, Austria, Belgium, Brazil, Germany, and Spain.

of M giants is self-excited (Mira-type) pulsations or stochastic (Solar-type) oscillations is still not clear (e.g. Dziembowski et al. 2001; Christensen-Dalsgaard et al. 2001; Bedding et al. 2005).

In this context, Tabur et al. (2010) showed that, as we advance through the RGB, the observed low amplitude of stochastically excited solar-type oscillations, typical of the GK-type giants, progress to a mixture of Mira-like and solar-like variability, as found in SR variables, and ending with stable, mono-periodic, Mira-like pulsations. Afterwards, Mosser et al. (2013), studied global oscillation parameters of *Kepler* red giants, concluding that the main excitation mechanism in M Giant SR variables are solar-like oscillations, confirming the findings by Dziembowski & Soszyński (2010), but could not disentangle RGB from AGB stars. Bányai et al. (2013) performed a detailed study of the variability of M-type giants using *Kepler* data as well. They affirm they could distinguish between solar-like oscillations and larger amplitude pulsations. They found a correlation of solar-like oscillations with period that closely follows the well-known v_{max} amplitude scaling relations (e.g. Mosser et al. 2010; Huber et al. 2011; Mosser et al. 2013), but they found a sharp ending to this correlation at $\log P \sim 1$. This feature may be an indication that a different excitation mechanism dominates from this point forward. Does this point mark the transition between solar-like and Mira-type pulsations? In their diagram, the stars classified as having a few periodic components (Miras and SRs) then follow a trend with a steeper slope, for $\log P$ greater than 1. This trend is similar to the one found by Tabur et al. (2010) for bright M-giant stars, depicting overtone pulsators, with a few stars following the fundamental mode trend (typical of Mira-type stars) as well.

Another point of discussion concerns the observation of rapid variations of brightness on time-scales between 3 minutes to 30 days in long period variables (hereafter LPVs) (e.g., Schaefer 1991; Maffei & Tosti 1995; de Laverny et al. 1998). However, these events were not confirmed in recent studies (e.g., Mais et al. 2004; Woźniak et al. 2004; Lebzelter 2011; Hartig et al. 2014). Indeed, Lebzelter (2011) and Hartig et al. (2014), using data from CoRoT and *Kepler*, did not confirm such variations, despite photometric precisions of the order of a few mmag. Therefore, the observed short-time variations are very rare or not physical.

In this study we perform a comprehensive analysis of the variability of M-giants observed by CoRoT, and we compare our results with previous studies regarding the variability behavior of M-giant stars observed by others authors. The paper is structured as follows. In Sect. 2, we describe our working sample and our catalog. In Sect. 3, we present our results and compare them with previous works from the literature. We also investigate the difference between CoRoT stars located towards the inner and outer regions of the Galaxy. Finally, in Sect. 4, we present our conclusions and discuss future perspectives.

2. Working Sample

The CoRoT satellite was launched in 2006. It collected point-source photometric data towards inner (around RA = 18h50m, Dec = +00°) and outer (around RA = 06h50m, Dec = +00°) regions of the Galaxy over a period of 6 years. A total of 162 789 sources were observed, with 5762 classified as M-type stars (Deleuil et al. 2009). These stars constitute approximately 4% of all stars observed by CoRoT and are divided in two main groups: giants (luminosity classes I, II, and III) and dwarfs (luminosity class V). giants comprise approximately 44% of all M-type stars detected by CoRoT, whereas the percentage of M dwarfs is ap-

proximately 56%. A total of 973 M-type stars were observed at least twice, providing a unique sample for studying long-term photometric variations. Table 1 lists the number of M-type stars observed with CoRoT towards the inner (center) and outer (anti-center) regions of the Galaxy.

CoRoT Region	I	II	III	V
Center	136	189	1339	1807
Anticenter	48	31	791	1421

Table 1. CoRoT M-type stars taken from EXO-Dat (Deleuil et al. 2009) distributed by luminosity class.

The latest CoRoT data release N2¹ provides light curves (LCs) that are corrected for instrumental noise cause by electronic, background and jitter sources. The effect of the South Atlantic Anomaly (SAA) passage was also included, and hot pixels of the detector are now flagged (Auvergne et al. 2009). At the time of the beginning of this work, the data were not yet completely corrected and some problems remained in the released data, requiring further treatment before the data was ready for analysis. In particular, the data contained long-term trends produced by CCD temperature variations, jumps (discontinuities) produced by hot pixels, and outliers (Auvergne et al. 2009). The post-processing of the LCs performed in different works follows different methods, according to the objectives of the works (e.g., Renner et al. 2008; Basri et al. 2011; Affer et al. 2012; De Medeiros et al. 2013), and thus far, there is no standard method to analysed the processed data. In the present work, we followed the general guidelines presented by De Medeiros et al. (2013).

First, we selected all sources classified as M-type giant stars in the CoRoT database. This first pre-selection, which yielded 2534 objects, provided us with a reasonable of actual giants, although the luminosity class specified in the CoRoT database is sometimes incorrect.

We also obtained the Harris V and Sloan-Gunn r' and i' photometry from the Exo-Dat catalog (Deleuil et al. 2009) and JHK_s photometry from the Two Micron All Sky Survey (2MASS- Skrutskie et al. 2006) catalog. The indexes V , r' , and i' were transformed into Johnson V and I -band photometry using the relations in Deleuil et al. (2009), with propagation of the respective errors.

Then, we dereddened the photometry using the extinction coefficients A_V , A_I , A_J , and A_K calculated with the relations from Schlafly & Finkbeiner (2011) and $E(B-V)$ reddening maps taken from Schlafly et al. (2014). We took the uncertainties from the coefficients and reddening maps and propagated them to obtain the final uncertainty of the corrected photometry. The transformed Johnson photometry and the unreddened photometry are listed in Tables 2 and 3.

2.1. Cross-identification

We performed a systematic cross-check of the 2534 M-giants to identify previous studies in the literature. To this end, we used the SIMBAD database², the General Catalog of Variable Stars (Samus et al. 2012), the AAVSO International Variable Star Index (VSX v1.1, now including 325,346 variable stars; Watson et al. (2014)), the New Catalog of Suspected Variable

¹ <http://idoc-corot.ias.u-psud.fr/>

² <http://simbad.u-strasbg.fr/simbad/>

Stars (Kazarovets et al. 1998), the Northern Sky Variability Survey catalog (NSVS; Hoffman et al. 2009), and a few catalogs of carbon stars (MacConnell 1988; Stephenson 1989, 1996; Alksnis et al. 2001; Chen & Yang 2012; Zacharias et al. 2013). We also cross-checked with previous studies using CoRoT data (Lebzelter 2011; Sebastian et al. 2012; Guenther et al. 2012; Sarro et al. 2013; De Medeiros et al. 2013). Finally, we also searched in many other databases incorporated in the International Virtual Observatory Alliance³, using the Tool for Operations on Catalogues And Tables (TOPCAT)⁴. The search assumed a positional accuracy of 2'' in the sky coordinates.

A total of 465 stars were in common with other studies. Among them there are 390 semi-sinusoidal variables, 45 LPVs, 14 Orion type variable stars, 8 Carbon stars, 6 Mira type stars, 4 binary systems, 2 pre-main sequence stars, 2 high proper-motion stars, 1 Delta Scuti star, and 1 Gamma-Doradus star. Some of these stars have more than one classification. For instance, 15 semi-sinusoidal variables are also classified as LPVs. At the same time, not every star has a known period. The Orion type, Gamma-Doradus, and pre main-sequence stars, as well as stars in binary systems were withdrawn from our sample. The remaining sources were used to compare our period measurements (see Sect. 2.3). The stars in common with the literature depicting their variability types are presented in the column 2 of Tables 2 and 3).

2.2. Effective temperature estimation

The T_{eff} values of the M-giants were calculated using the photometric-effective temperature relation of van Belle et al. (1999),

$$T_{\text{eff}} = 3030 + 4750 \times 10^{-0.187(V-K)} \text{ K.} \quad (1)$$

Such a procedure was chosen to provide a homogeneous set of T_{eff} estimations. This is a precise tool directly based on interferometric measurements.

The effective temperature was calculated using the unreddened V- and K-band photometry. We transformed the K_S magnitudes to K_{CIT} photometry using the relation of Carpenter (2001) and calculated the T_{eff} values. The K_{CIT} photometry was used because it is the closest band to the one that was used to establish the original calibration (van Belle, private communication).

The uncertainties in the T_{eff} values were estimated by propagating the errors of the corrected magnitudes and the K_S transformation uncertainty. Then, we added the photometric uncertainty in quadrature to the estimated errors from Table 8 of van Belle et al. (1999), taking the maximum error of the two $V - K$ bins that were closest to each parameter value. The results are presented in Table 2.

2.3. Variability analysis

A Lomb-Scargle periodogram (Lomb 1976; Scargle 1982) was computed for each LC, except for the LPV candidates (C3 - see Sect. 2.4). We set the low-frequency limit (f_0) for each periodogram to be $f_0 = 1/T_{\text{tot}}$, where T_{tot} is the total time spanned by the LC. The high-frequency limit was fixed to $f_N = 10 \text{ d}^{-1}$, and the periodogram size was scaled to 10^4 elements. The highest periodogram peak, which is referred to as frequency f_1 or period

P_1 , was refined following De Medeiros et al. (2013), namely, by maximizing the ratio of the variability amplitude to the minimum dispersion given by Dworetzky (1983). Next, the refined frequency f_1 was used to calculate a harmonic fit with two harmonics. This fit was used as a model to compute the mean variability amplitude (A) in units of magnitude (mag), and is defined as

$$y(t) = \sum_{j=1}^2 [a_j \sin(2\pi f_1 j t) + b_j \cos(2\pi f_1 j t)] + b_0, \quad (2)$$

in the phase diagram of the main period, where f_1 is the frequency, a_j and b_j are the Fourier coefficients, t is the time and b_0 is the background level.

For our M giants (typically stars with $T_{\text{eff}} < 4200 \text{ K}$ - see Sect. 2.4), we defined the variability amplitude as the half of the difference between the maximum and minimum of Eq. 2 in the phase diagram of the main period, which is similar to the amplitude definitions used by De Medeiros et al. (2013) and Bányai et al. (2013). This fit was then applied to the LC domain and was subtracted from the time series (prewhitening), thereby yielding a new Lomb-Scargle periodogram. The procedure was iterated N times; in each iteration, the LCs were fitted with a harmonic fit using two harmonics. For each LC, we selected all the independent periods that exhibited a significance level greater than 99%, i.e., a false alarm probability (FAP) less than 0.01. Therefore, a collective set of independent periods for each target was retained to perform an analysis that was similar to that of Tabur et al. (2010) and Bányai et al. (2013) (see results presented in Sect. 3). The FAP was computed based on the Eaton et al. (1995) method, which consists of randomizing the temporal bins of the original LC and computing the resulting power spectra (see also Affer et al. 2012). We produced 1000 modified LCs for each period by randomizing the positions of blocks of adjacent temporal bins, with a block length of 12 hours, in accordance with Affer et al. (2012). Regarding our semi-sinusoidal sources with $T_{\text{eff}} > 4200 \text{ K}$ (C2 - see Sect. 2.4), we performed the analysis once and keep only one period and amplitude (see Table 3). This process was iterated N times for C1 stars, considering the first three periods above the FAP, to study the multi-modes which are displayed in Table 2, where we present the photometric information for the LPV candidates (see Table 4).

A total of 434 stars with previously determined periods (Lebzelter 2011; De Medeiros et al. 2013) were found. For approximately 96% of the targets, the differences between our periods and the other authors are less than 10%. We attribute the differences to four main reasons: first, the pipeline improvements made by the CoRoT team now result in better data for analysis; second, the combination of all observations provides a wider time window and thus more precise periods; third, detrending of long-term variations may misshape a small portion of the LCs; and fourth, the first harmonic may be falsely identified as the main frequency when there are too few cycles, as explained in De Medeiros et al. (2013). The precision of the analysis of the nature of the variability, period, and amplitude increases with the number of cycles (the ratio of total time span to the variability period), as discussed in De Medeiros et al. (2013). According to those authors, for the CoRoT LCs, the variability periods with more than three cycles have a confidence level of greater than 80%. The photometric instrumental jumps in the CoRoT data also hinder the analysis of potential long-period variability.

³ <http://www.ivoa.net/>

⁴ <http://www.star.bris.ac.uk/~mbt/topcat/>

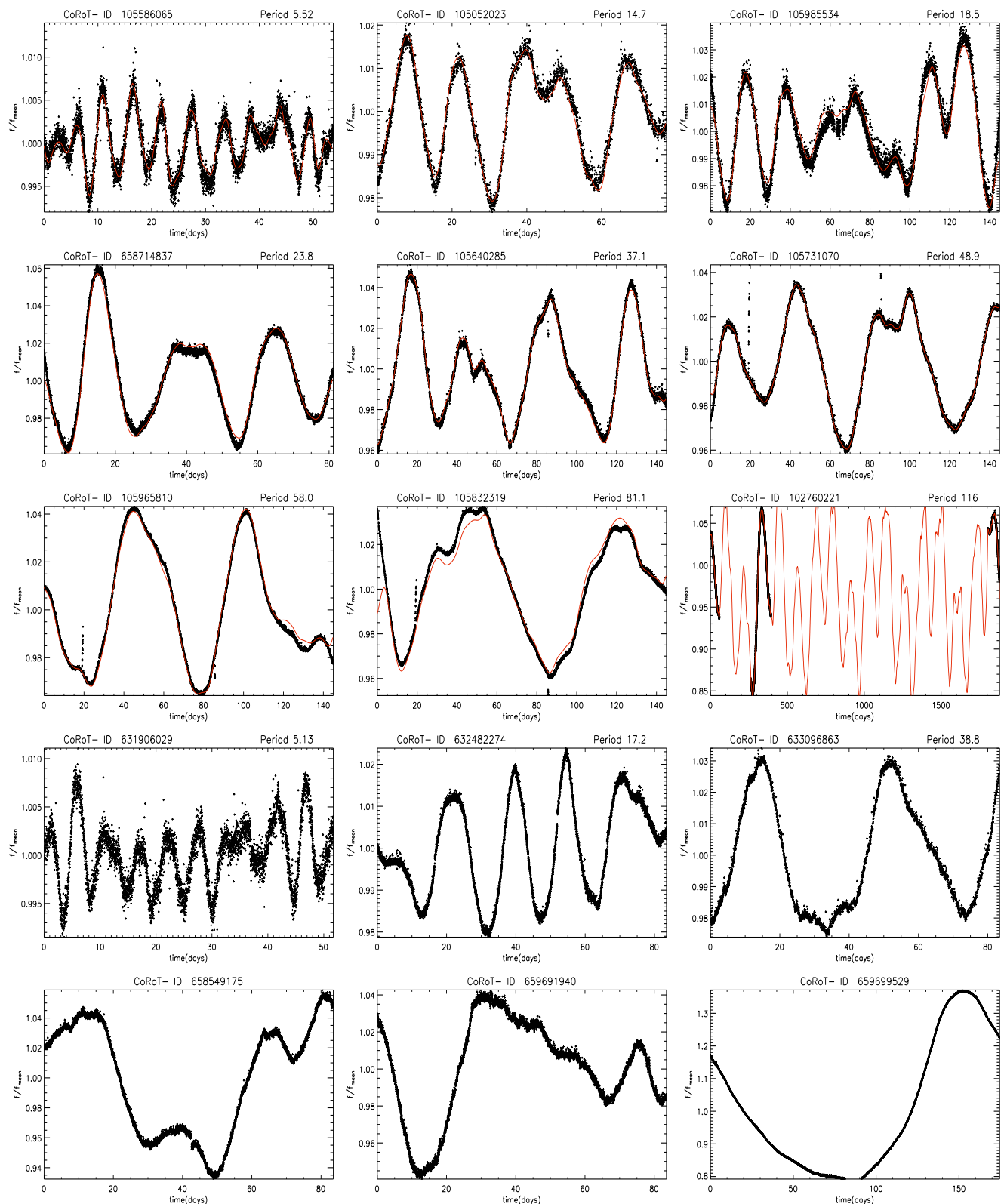


Fig. 1. Typical LCs of stars from our catalog. CoRoT-ID and period of the C1 (row 1-3) and C2 (row 4) catalogs are shown in the headers. For the C3 (LPVs - row 5) sources only the CoRoT-ID is shown. The red line marks the harmonic fit models of the C1 stars given by Eq. 2.

2.4. The CoRoT M stars variable catalogue

Our final sample is composed of all semi-sinusoidal variable stars and long period variables candidates in the CoRoT database

that were classified as M-giants (1428 stars). This catalogue is composed of three main groups: A - 1173 semi-sinusoidal variables with $T_{\text{eff}} \leq 4200$ K; B - 141 semi-sinusoidal variables with $T_{\text{eff}} > 4200$ K; C - 114 LPVs candidates (from which 105 have

$T_{\text{eff}} \leq 4200$ K, 4 have $T_{\text{eff}} > 4200$ K, and 5 do not have either V or K -band photometry). The cutoff of $T_{\text{eff}} < 4200$ K was performed to exclude targets that could be misclassified as M-type.

Fig. 1 presents LCs with typical C1 (rows 1-3), C2 (row 4), and C3 (last row) signatures. CoRoT-102760221 (right panel of the third row) shows a combination of CoRoT runs that provides a wider time window, used to search for longer-periods variations. Tables 2, 3, and 4 present the properties of the C1, C2, and C3 sub-catalogs, respectively. Columns 1 to 10 depict the CoRoT ID, right ascension declination, time window of the CoRoT run, spectral type, luminosity class, B, V, J, H, and K_s magnitudes. Columns 11 to 13 show the computed periods, variability amplitudes, and T_{eff} values, for the stars contained in Tables 2 and 3. The period distribution ranges from ~ 2 to ~ 150 day, with a maximum around ~ 17 day. The variability amplitudes range from ~ 1 to ~ 900 mmag, with a maximum of approximately ~ 10 mmag.

The C1 and C3 sources are used to describe the evolutionary and variability behavior of M-Giant type stars in forwards sections.

3. Results

We report our results in the following subsections, using a final sample of 1314 M-giants (C1 and C3 stars). First, we perform an analysis of the $V-I$ versus $J-K$ color diagram, and compare our results to the models of Aringer et al. (2009) and the empirical calibrations of Worthey & Lee (2011), and to other works from the literature. Then we discuss and interpret our results using the period-amplitude and the period- T_{eff} diagrams. Afterwards we compare the results of the measured period and amplitude from the stars located towards the inner and outer regions of the Galaxy. Finally, we discuss the lack of short-time variations in M giants, and make a brief mention on the Mira Variable stars and the Carbon stars we have in common with other works.

3.1. The evolutionary behavior along the color-color diagram

Figure 2 shows the color-color diagrams of our C1 (full circles) and C3 ($T_{\text{eff}} < 4200$ K - 105 stars) (full triangles) sub-samples where the colors set the spectral type (upper panel) and luminosity class (lower panel). Here we only consider stars with V , I , J and K -band photometry. The error bars in the bottom right corner of the two diagrams represent the typical uncertainties for the colors ($\epsilon_{(V-I)} = 0.29$ dex and $\epsilon_{(J-K)} = 0.09$ dex). The red and blue circles around some targets represent stars belonging to the anticenter fields and the center field LRC03 respectively. The black squares depict previously identified carbon stars, taken from the literature. The photometric calibrations of Worthey & Lee (2011) are depicted by three dashed-dotted black lines, corresponding to iso-gravity contours, from left to right, of $\log g = 3, 2$ and 0 dex. The small black dots represent the hydrostatic models of carbon giants from Aringer et al. (2009). We note that the reddening may not only be caused by interstellar but also by circumstellar reddening (Lebzelter 2011).

The corrected colors show a reasonable agreement with the empirical calibrations of Worthey & Lee (2011). However, there are two groups of stars that do not follow this trend. One group, with a lower average value of $V - I$ situated between the photometric calibrations and the synthetic photometry from hydrostatic models of C-rich giants from Aringer et al. (2009). Nevertheless, only an abundance analysis would allow us to determine if these targets are Carbon stars. Interestingly, almost

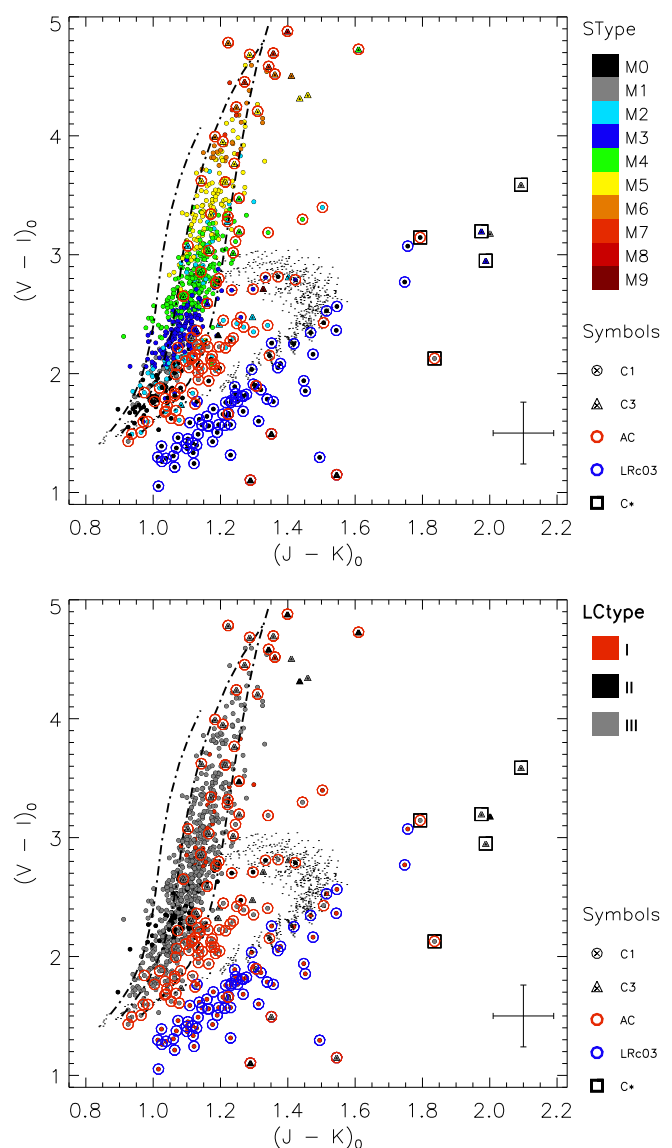


Fig. 2. $V - I$ vs $J - K$ color-color diagram of C1 (circles) and C3 (triangles) subsamples. The colors indicate the spectral type (upper panel) and luminosity class (bottom panel). The dashed-dotted lines display the dereddened location of M-giants according to Worthey & Lee (2011). The small black dots mark the location of hydrostatic Carbon stars from the models by Aringer et al. (2009). The stars previously classified as Carbon stars are depicted by a square symbol. The stars from the samples towards the outer regions of the Galaxy are marked by open red circles while the stars from the LRC03 CoRoT Run are identified using blue open circles. The error bars in the bottom right corner of the two diagrams represent the typical uncertainties for the colors ($\epsilon_{(V-I)} = 0.29$ mag and $\epsilon_{(J-K)} = 0.09$ mag)

all stars from this sub-group belong to the CoRoT anticenter fields. We do not know the reason of this behaviour, but we hypothesise that the samples towards the inner and outer regions of the Galaxy may belong to two different Galactic populations. In fact, an increasing trend of the C star/M star ratio with $[\text{Fe}/\text{H}]$ in the Galaxy is reported in the literature (e.g Frebel et al. 2006) and in the Large Magellanic Cloud (Blanco et al. 1980; Cioni & Habing 2003). At the same time, a negative trend with $[\text{Fe}/\text{H}]$ has been reported by different studies (e.g Boeche et al. 2013; Bergemann et al. 2014), at low values of Galactic vertical

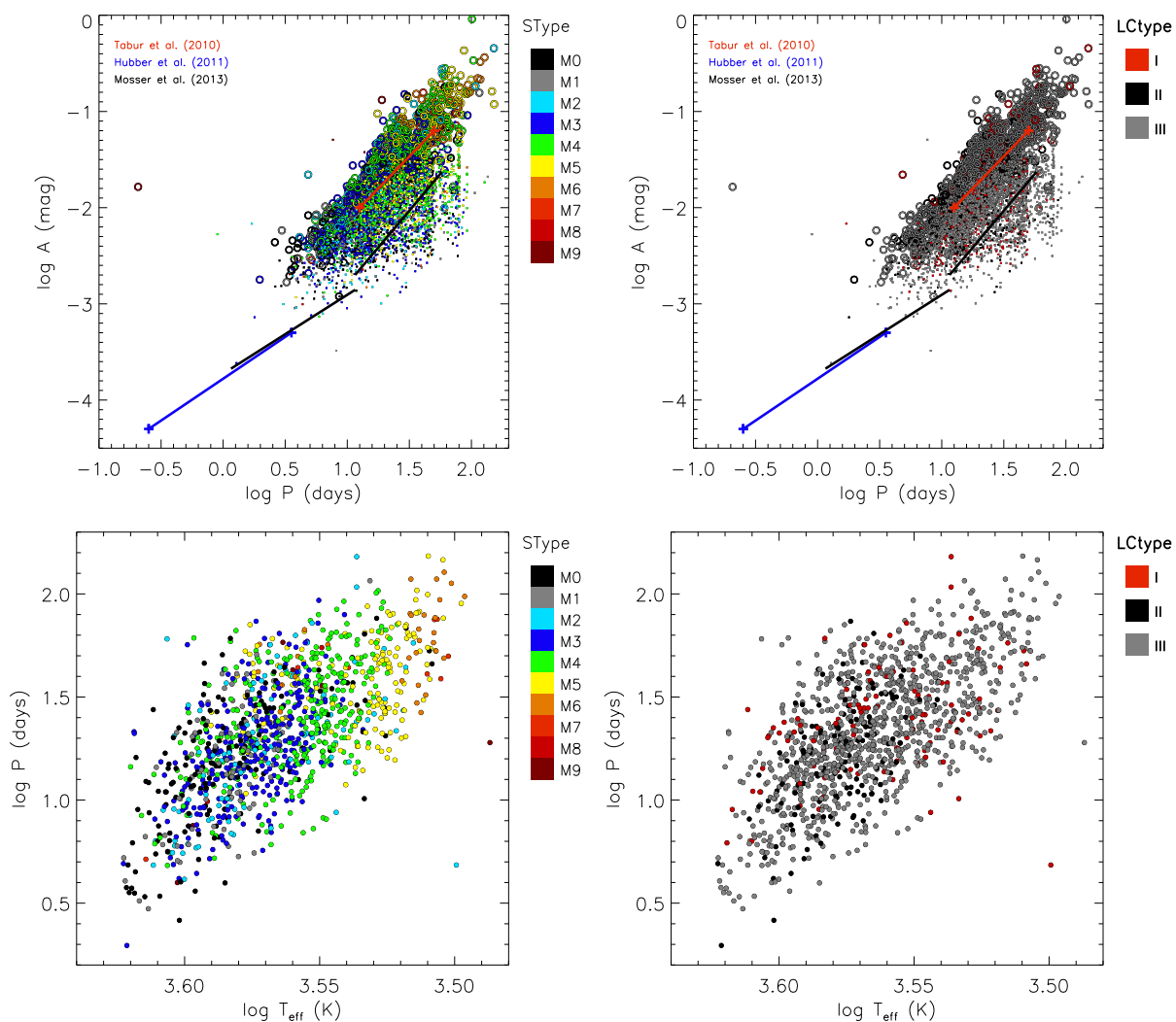


Fig. 3. The distribution of variability period as a function of the amplitude and the effective temperature for C1 stars. The colors indicate the spectral type (left panels) and luminosity class (right panels). The large circles in the upper panels mark the main variability period and the small circles mark the secondary periods. In the lower panels only the main variability period is shown. The red line between the two red crosses roughly depict the trend of the overtone (AB) pulsators taken from Fig. 15 of Tabur et al. (2010). The blue line between the two blue crosses represent the area defined by Bányai et al. (2013), selected from the top panel of Fig. 3 of Huber et al. (2011), where is expected to find solar-like oscillations. The two black lines describe the two distinct Amplitude- ν_{max} relations for solar-type oscillators found by Mosser et al. (2013) (their Equations 8 and 9).

height ($|Z| < 300 - 400$ pc). Therefore, a possible explanation for the imbalance of C stars between the two fields may be related to the negative $[\text{Fe}/\text{H}]$ trend as a function of the Galactic Radius. Our results are in close agreement with those presented in Fig. 2 of Lebzelter (2011).

We also observe that most of the super-giant population (Type I) has a lower value of $V - I$ for the same $J - K$ color, when compared to the two groups of Giant stars, and are located below the predicted region for C-rich stars. For $J - K > 1.3$ the location of these stars coincide with the models, but theoretical traces from Aringer et al. (2009) do not cover spectral class I.

The LPVs Candidates (C3 catalog) are distributed throughout the color-color diagram. This is expected since the time span of the LPVs range from 24 to 145 day, implying a greater variability period. Eight of twelve stars with $V - I > 3.8$ have a total time span greater than 100 day (and therefore a greater period). These aspects agree with the period versus T_{eff} trend (Fig. 3 lower panels) since we expect long periods for stars with lower

temperatures (and higher $V - I$ color). This result strongly suggests that long-term trends found for all LPVs candidates may be real.

3.2. The period variability and amplitude behavior

To investigate the nature of the stellar photometric variability identified in the present work, we studied the period variability as a function of amplitude and effective temperature for stars of the present sample that exhibit semi-sinusoidal behavior in their observed LCs. For such a purpose, we have used the periods and amplitudes for the sample of 1173 stars described in Sect. 2.4 (the C1 catalog). To study the multi-mode behavior we considered the first three independent frequencies on the period-amplitude diagrams of Fig. 3. In the case of the T_{eff} -period diagrams, we only used the main period.

The distribution of the multi-modes as a function of the amplitude is displayed in Fig. 3 (upper panels). The circles repre-

sent the stronger mode, while the dots depict the other modes of oscillation. The red line between the two red crosses roughly depict the trend of the overtone (AB) pulsators taken from Fig. 15 of Tabur et al. (2010). The blue line between the two blue crosses represent the area defined by Bányai et al. (2013), selected from the top panel of Fig. 3 of Huber et al. (2011), where is expected to find solar-like oscillations. The two black lines describe the two distinct Amplitude- ν_{max} relations for solar-type oscillators found by Mosser et al. (2013) (their Equations 8 and 9).

The observed period-amplitude behavior clearly parallels the classical scenario for the pulsation period-amplitude relation which has been well established for M-giant stars with semi-sinusoidal variations using different stellar samples observed from the ground (e.g., Alard et al. 2001; Wray et al. 2004; Tabur et al. 2010).

The scenario presented in Fig. 3 (upper panels), for the stronger pulsation (open circles), follows closely the trend observed by Tabur et al. (2010) (red line in the Diagram), which corresponds to stars pulsating in overtones. The other modes of oscillation agree well with the Amplitude- ν_{max} relation of Mosser et al. (2013), for $\nu < 1\mu\text{Hz}$, corresponding to $\log P > 1.06$ day. The two distinct relations suggest the presence of two different oscillation mechanisms: the stronger one, characteristic of self-excited Mira-like pulsations; the smaller amplitude ones, mimicking the behavior of solar-type oscillations.

Our finding also agrees with the results of Bányai et al. (2013), who, on the basis of *Kepler* observations of M-giant stars (their group 3), found a similar period-amplitude behavior. Group 3, as defined by those authors, contains stars with LCs that exhibit only a few periodic components (like Miras and SRs) that are in agreement with the signatures of semi-sinusoidal variables. Bányai et al. (2013) also reported a sharp break at $\log P \sim 1$ day (corresponding to $1.2\mu\text{Hz}$), marking the end of the clear correlation between their Group 2 and their adapted relation from Amplitude- ν_{max} relation of Huber et al. (2011). We do not observe a trend in our Fig. 3 (upper panels) in the same region of $\log P$. However, we must note we have very few periods with similar amplitudes in that Period region. Despite that, if we account only the stronger pulsation we observe, by eye, that there is a slight change of slope around $\log P \sim 1$ day.

We also analyzed the relation period- T_{eff} . Fig. 3 (lower panels) shows all 1141 giant stars from our C1 sample with semi-sinusoidal variations, where only the primary computed pulsation period is considered. We observe a correlation of the period of the main oscillation with T_{eff} similar to the trend found by Huber et al. (2011) for hotter giants from the *Kepler* sample, with the oscillation frequency ν_{max} . A careful comparison of our Fig. 3 (bottom left panel) with Fig. 8 of Huber et al. (2011), points for an agreement between both trends. Indeed, the feature revealed from Fig. 3 (lower panels) seems to correspond to an extension of the upper part of the modified H-R diagram (Figure 8) of Huber et al. (2011).

3.3. The inner and outer regions of the Galaxy

To verify whether the behavior of the variability of sources from the inner and outer regions of the Galaxy are significantly different, we applied the Kuiper test (or invariant KS test - hereafter the KS test) (e.g. Jetsu & Pelt 1996; Paltani 2004) to our C1 subgroup. The C1 is composed of 1124 stars located toward inner and 91 in outer regions of the Galaxy. According to the KS test, zero probability means that the distributions are dissimilar, whereas unit probability means they are drawn from the same parent distribution.

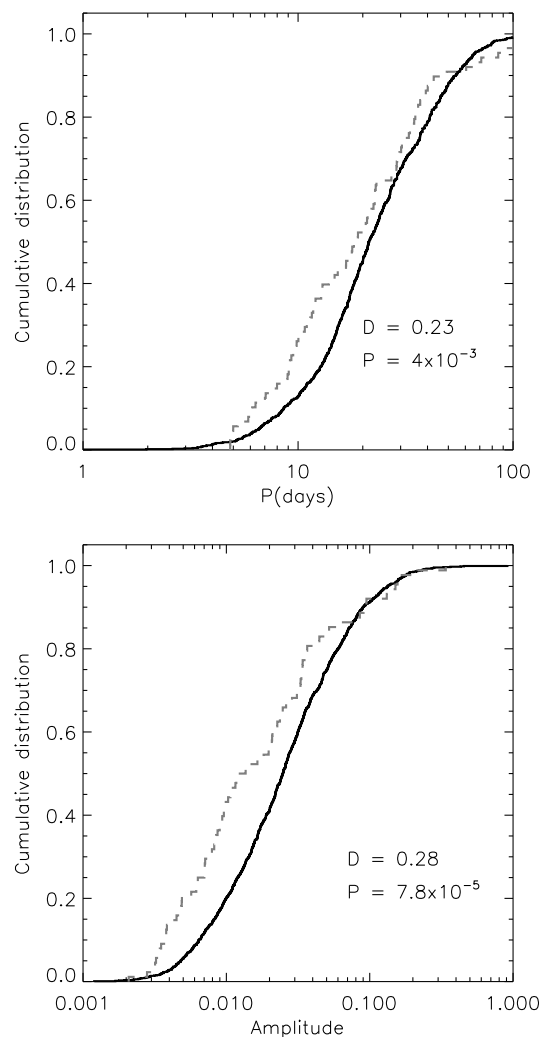


Fig. 4. Cumulative distribution function of the period (left panel) and amplitude (right panel) for stars at the inner (solid line) and outer (dashed line) regions of the Galaxy.

Figure 3.3 shows the cumulative distribution function of the amplitude and period of C1 stars. The solid black distribution depicts the stars located in the inner regions whereas the dashed grey distribution describes the outer region. The obtained p-values for the amplitude and period distributions are lower than 10^{-3} . This result shows that there is a very low probability that the two samples belong to the same parent distribution. The difference between the two samples may also be observed in the color-color diagram (Fig. 2) where most stars from the outer region sample are in the region commonly associated with Carbon stars, while the sample from the inner region of the Galaxy are mostly M giants. Also, the metallicity of our two samples should be different (see Sect. 3.1) and this may play an important role on M Giant evolution, since these distributions are dissimilar in terms of amplitude and period.

We tested the KS test by perturbing our two samples. First, we withdrew a random quantity of stars from our sample between 5% to 10% using an uniform Monte Carlo distribution and next we performed the KS test. The process was iterated for 1000 times. The higher 3σ value taken from the median of the amplitude and period distribution was 0.002 and 0.05 respec-

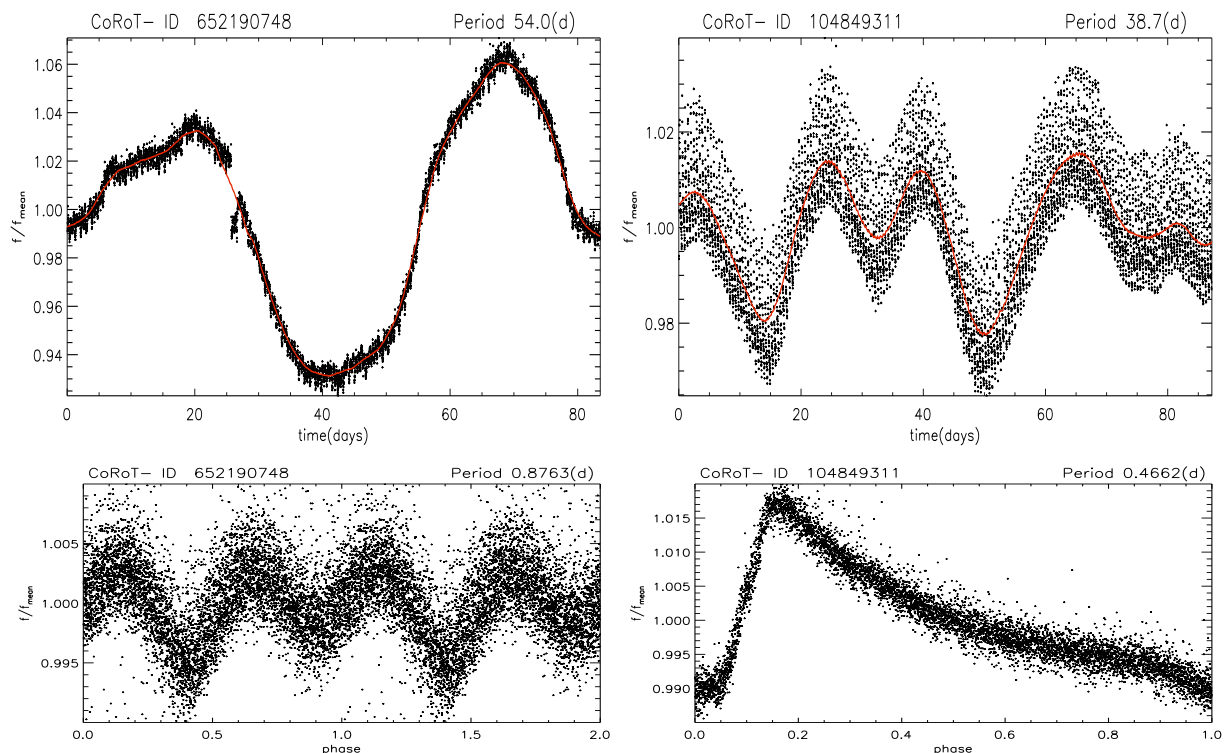


Fig. 5. CoRoT 652190748 and CoRoT 104849311 light curves (upper panels). The red line displays a boxcar smoothed version of the LC. The phase diagrams of their short time variations are depicted in the lower panels. The CoRoT-ID and period are presented in each panel.

tively. The indicative of dissimilarity is not robust enough for the period distribution.

3.4. Short-time variations of CoRoT M-giant stars

The CoRoT data have at least a 512 second sampling interval and a long coverage period that allow us to study the occurrence of rapid outbursts or very short time variations in LPVs on very short time scales (from hours to a few days). These variation changes of several tenths of magnitudes should occur once per star per year according to the literature (Woźniak et al. 2004). A recent study using a sample of 52 CoRoT stars (Lebzelter 2011) and 9 *Kepler* stars (Hartig et al. 2014) presented no detections of such rapid variations for amplitudes above 0.01 mag. However, only a small number of sources was analysed.

A detailed search by visual inspection on the LCs of all CoRoT M giant stars composing the present sample, did not yield any short term event. All outburst-like variation found may be related to hot pixel events or other instrumental artefacts (check, for instance, the LC panels of CoRoT 105731070, 105832319, and 105965810 of Fig. 1). This agrees with other recent studies showing that this phenomenon is rare or does not exist (e.g., Woźniak et al. 2004; Lebzelter 2011; Hartig et al. 2014). Taking into account all results from different instruments and small and large samples, we can conclude that the short-time outbursts (< 1 day) in long-period variables do not exist or at least are very rare events.

Another possible cause of a false outburst event may lie with a background star. In this case, the observed variation will be the superposition of the signal from both stars. Fig. 5 shows two CoRoT LPVs where the phase diagrams (lower panels) show a signature of a background binary (left panel) and a RR-Lyrae (right panel) star. To study the short time variation of the two

LCs, a prewhitened curve was obtained by dividing each LC by a boxcar smoothing function of the curve itself. Then, the period was computed using a similar procedure such as described in Sect. 2.3.

3.5. Long Period Variables

Three LPVs stars of our sample were previously analyzed by Lebzelter (2011) using CoRoT data. Some of these stars are also common to the AAVSO International Variable Star Index (Watson et al. 2014) catalog. In the present LPVs sample (C3) we identify four Mira variable stars, CoRoT 104982243, 105580931, 632685506, and 653546843, with previously computed periods of 329, 205, 195, and 116 day respectively (Watson et al. 2014).

3.6. Carbon Type Stars

Eight carbon type stars, previously described in the literature (MacConnell 1988; Stephenson 1989, 1996; Alksnis et al. 2001; Chen & Yang 2012; Zacharias et al. 2013; Watson et al. 2014), are identified in our sample. These stars are in the fields towards the outer regions of the Galaxy (LRa01, IRa01, and LRa02 CoRoT runs). The combination of different CoRoT Runs allow us to study the long periods of the Carbon stars with more accuracy. For instance, CoRoT-ID 102760221 (see Fig. 1 last row, right panel) was analysed by Lebzelter (2011) using the CoRoT Runs IRa01 and LRa01. A period of 116 days is reported by Lebzelter (2011) as the probable main period once its LC present a minimum and a maximum between 250 and 400 days. Because the referred star was re-observed during the LRa06 Run, we have combined all the observations (CoRoT Runs IRa01, LRa01 and

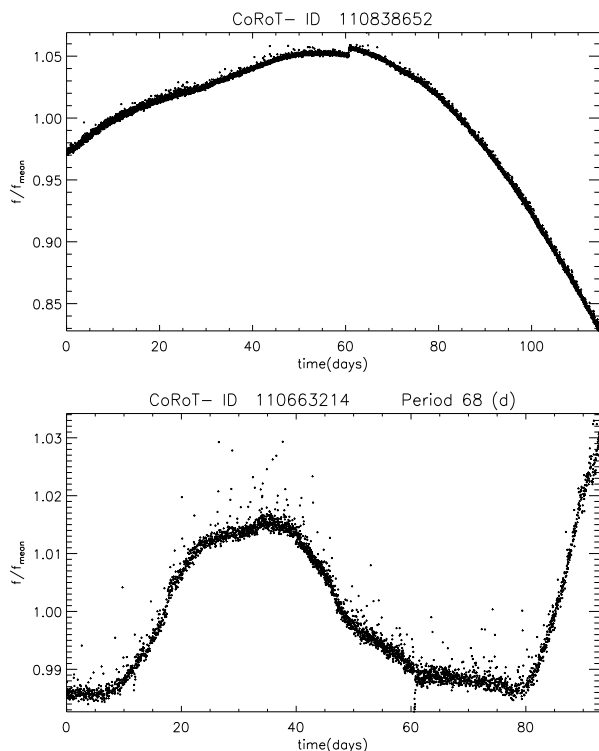


Fig. 6. LCs of two previously identified carbon type stars: CoRoT 110838652 and 110663214.

LRa06) for a check of the period measurements, finding now a period of 349 days, which may be related with the fundamental pulsation mode.

On the other hand, in some cases, the total time span is not long enough to provide a reliable period (see Fig. 6, upper panel) while in other cases we can observe more than one cycle (Fig. 6, lower panel). For instance, the star CoRoT 110663214 displays a period of 68 day. However, the shape of its LC indicates the existence of a larger period. Using the methodology of De Medeiros et al. (2013) we obtain a confidence level of about 70% for this period.

4. Conclusions

In this work we perform a study of the semi-sinusoidal variability behavior of CoRoT M-giant stars. This is the largest detailed study of M-giants observed by CoRoT, and it provides an opportunity for comparison with previous works based on space missions like CoRoT and *Kepler* (e.g. Lebzelter 2011; Bányai et al. 2013; Huber et al. 2014; Hartig et al. 2014) and on ground-based observations (e.g., Alard et al. 2001; Wray et al. 2004; Tabur et al. 2010).

We also present a CoRoT variability list for M-giant stars. The C1 sample, which contains 1173 objects, is composed of all stars classified as M-giants in the CoRoT database with $T_{\text{eff}} < 4200$ K. They were identified via visual inspection as semi-sinusoidal variables. The effective temperature T_{eff} was estimated from the calibration of van Belle et al. (1999) using $V - K$ color indices. The main variability period spans from ~ 2 to ~ 152 day, with the amplitude ranging from ~ 1 to ~ 900 mmag. The C2 sample is comprised of 141 stars that exhibit semi-sinusoidal variations (with $T_{\text{eff}} > 4200$ K), and the C3 sample contains 114 LPV candidates. The two last sub-samples

may be considered for follow-up observations to study their variability nature.

We performed a cross-check of our data with previously published catalogs and found 444 targets in common. The computed periods are similar (i.e., discrepancy less than 10%) for 96% of these targets, which indicates a good agreement between our results and previous results from the literature. The cross-matched sources were used to withdraw misclassification and to identify comparison stars.

The location of the majority of the sample stars in the $V - I$ versus $J - K$ color-color diagram shows a good agreement with the empirical calibrations of Worthey & Lee (2011). Two groups of stars present different trends. The first one, with a lower average value of $V - I$ for the same $J - K$ is mostly composed with stars from the outer region sample and is located between the Giant calibrations and the Carbon star models of Aringer et al. (2009). The second group, located in the lowest $V - I$ region of the diagram, appears to be mostly composed by a Type I supergiant population. The large majority of the stars from this group belong to the LRc03 field, towards the inner regions of the Galaxy.

We considered the first three periods with significance levels greater than 99% to study their behavior in a period-amplitude diagram. The distribution exhibits a trend of increasing amplitude with increasing period, which is compatible with the expected behavior for stellar pulsation (e.g., Alard et al. 2001; Wray et al. 2004; Tabur et al. 2010). We also observe that the main variability period follows closely the stars identified by Tabur et al. (2010) as overtone pulsators. The less powerful periods follow the trend formulated by Mosser et al. (2013) for solar-like oscillations. A similar analysis was performed using a period versus T_{eff} diagram, which exhibits a trend of increasing period with decreasing temperature. This trend is compatible with a previous study based on *Kepler* observations for GK giants (Huber et al. 2011), and our new data confirms that the behavior of the period-effective temperature relation extends to the cooler M-giant stars.

Regarding the short-time variations on M-giant stars previously reported in the literature, we also concluded that they do not exist or are very rare. The few cases we found are related to biases or background stars.

Acknowledgments

We would like to thank Evelin Banyai for useful discussions. Research activities of the Observational Stellar Board of the Federal University of Rio Grande do Norte are supported by the continuous grants of the CNPq and FAPERN Brazilian agencies and by the INCT-INEspaço. C. E. F. L. acknowledges a post-doctoral fellowship from the CNPq. F. P. Ch. acknowledges a doctoral fellowship from the CNPq. This research has made use of the NASA/IPAC Infrared Science Archive, which is operated by the Jet Propulsion Laboratory, California Institute of Technology, under contract with the National Aeronautics and Space Administration.

References

- Affer, L., Micela, G., Favata, F., & Flaccomio, E. 2012, MNRAS, 424, 11
- Alard, C., Blommaert, J. A. D. L., Cesarsky, C., et al. 2001, ApJ, 552, 289
- Alksnis, A., Balklavs, A., Dzervitis, U., et al. 2001, Baltic Astronomy, 10, 1
- Aringer, B., Girardi, L., Nowotny, W., Marigo, P., & Lederer, M. T. 2009, A&A, 503, 913
- Auvergne, M., Bodin, P., Boissard, L., et al. 2009, A&A, 506, 411

- Baglin, A., Auvergne, M., Barge, P., et al. 2007, in American Institute of Physics Conference Series, Vol. 895, Fifty Years of Romanian Astrophysics, ed. C. Dumitrache, N. A. Popescu, M. D. Suran, & V. Mioc, 201–209
- Bányai, E., Kiss, L. L., Bedding, T. R., et al. 2013, MNRAS, 436, 1576
- Basri, G., Walkowicz, L. M., Batalha, N., et al. 2011, AJ, 141, 20
- Batalha, N. M., Rowe, J. F., Bryson, S. T., et al. 2013, ApJS, 204, 24
- Bedding, T. R., Kiss, L. L., Kjeldsen, H., et al. 2005, MNRAS, 361, 1375
- Bergemann, M., Kudritzki, R.-P., & Davies, B. 2014, ArXiv e-prints
- Blanco, V. M., Blanco, B. M., & McCarthy, M. F. 1980, ApJ, 242, 938
- Boeche, C., Chiappini, C., Minchev, I., et al. 2013, A&A, 553, A19
- Borucki, W. J., Koch, D., Basri, G., et al. 2010, Science, 327, 977
- Borucki, W. J., Koch, D. G., Batalha, N., et al. 2012, ApJ, 745, 120
- Brown, T. M., Latham, D. W., Everett, M. E., & Esquerdo, G. A. 2011, AJ, 142, 112
- Carpenter, J. M. 2001, AJ, 121, 2851
- Chen, P. S. & Yang, X. H. 2012, AJ, 144, 104
- Christensen-Dalsgaard, J., Kjeldsen, H., & Mattei, J. A. 2001, ApJ, 562, L141
- Cioni, M.-R. L. & Habing, H. J. 2003, A&A, 402, 133
- de Freitas, D. B., Leão, I. C., Ferreira Lopes, C. E., et al. 2013, ApJ, 773, L18
- de Laverny, P., Mennessier, M. O., Mignard, F., & Mattei, J. A. 1998, A&A, 330, 169
- De Medeiros, J. R., Ferreira Lopes, C. E., Leão, I. C., et al. 2013, A&A, 555, A63
- Deleuil, M., Meunier, J. C., Moutou, C., et al. 2009, AJ, 138, 649
- Dressing, C. D. & Charbonneau, D. 2013, ApJ, 767, 95
- Dworetzky, M. M. 1983, MNRAS, 203, 917
- Dziembowski, W. A., Gough, D. O., Houdek, G., & Sienkiewicz, R. 2001, MNRAS, 328, 601
- Dziembowski, W. A. & Soszyński, I. 2010, A&A, 524, A88
- Eaton, N. L., Herbst, W., & Hillenbrand, L. A. 1995, AJ, 110, 1735
- Frebel, A., Christlieb, N., Norris, J. E., et al. 2006, ApJ, 652, 1585
- Guenther, E. W., Gandolfi, D., Sebastian, D., et al. 2012, A&A, 543, A125
- Hartig, E., Cash, J., Hinkle, K. H., et al. 2014, AJ, 148, 123
- Hekker, S., Elsworth, Y., Mosser, B., et al. 2013, A&A, 556, A59
- Huber, D., Bedding, T. R., Stello, D., et al. 2011, ApJ, 743, 143
- Huber, D., Ireland, M. J., Bedding, T. R., et al. 2012, ApJ, 760, 32
- Huber, D., Silva Aguirre, V., Matthews, J. M., et al. 2014, ApJS, 211, 2
- Jetsu, L. & Pelt, J. 1996, A&AS, 118, 587
- Kazarovets, E. V., Samus, N. N., & Durlevich, O. V. 1998, Information Bulletin on Variable Stars, 4655, 1
- Kiss, L. L. & Bedding, T. R. 2003, MNRAS, 343, L79
- Lanza, A. F., Das Chagas, M. L., & De Medeiros, J. R. 2014, A&A, 564, A50
- Lebzelter, T. 2011, A&A, 530, A35
- Lebzelter, T., Schultheis, M., & Melchior, A. L. 2002, A&A, 393, 573
- Léger, A., Rouan, D., Schneider, J., et al. 2009, A&A, 506, 287
- Lomb, N. R. 1976, Ap&SS, 39, 447
- MacConnell, D. J. 1988, AJ, 96, 354
- Maceroni, C., Montalbán, J., Michel, E., et al. 2009, A&A, 508, 1375
- Maciel, S. C., Osorio, Y. F. M., & De Medeiros, J. R. 2011, New A, 16, 68
- Maffei, P. & Tosti, G. 1995, AJ, 109, 2652
- Mais, D. E., Stencel, R. E., & Richards, D. 2004, Journal of the American Association of Variable Star Observers (JAAVSO), 33, 48
- McQuillan, A., Aigrain, S., & Mazeh, T. 2013, MNRAS, 432, 1203
- Morton, T. D. & Swift, J. 2014, ApJ, 791, 10
- Mosser, B., Belkacem, K., Goupil, M.-J., et al. 2010, A&A, 517, A22
- Mosser, B., Dziembowski, W. A., Belkacem, K., et al. 2013, A&A, 559, A137
- Nielsen, M. B., Gizon, L., Schunker, H., & Karoff, C. 2013, A&A, 557, L10
- Paltani, S. 2004, A&A, 420, 789
- Renner, S., Rauer, H., Erikson, A., et al. 2008, A&A, 492, 617
- Riebel, D., Meixner, M., Fraser, O., et al. 2010, ApJ, 723, 1195
- Sarro, L. M., Debosscher, J., Neiner, C., et al. 2013, A&A, 550, A120
- Scargle, J. D. 1982, ApJ, 263, 835
- Schaefer, B. E. 1991, ApJ, 366, L39
- Schlafly, E. F. & Finkbeiner, D. P. 2011, ApJ, 737, 103
- Schlafly, E. F., Green, G., Finkbeiner, D. P., et al. 2014, ApJ, 789, 15
- Sebastian, D., Guenther, E. W., Schafferoth, V., et al. 2012, A&A, 541, A34
- Silva Aguirre, V., Casagrande, L., Basu, S., et al. 2012, ApJ, 757, 99
- Skrutskie, M. F., Cutri, R. M., Stiening, R., et al. 2006, AJ, 131, 1163
- Slawson, R. W., Prša, A., Welsh, W. F., et al. 2011, AJ, 142, 160
- Soszyński, I., Dziembowski, W. A., Udalski, A., et al. 2007, Acta Astron., 57, 201
- Soszyński, I., Wood, P. R., & Udalski, A. 2013, ApJ, 779, 167
- Stephenson, C. B. 1989, Publications of the Warner & Swasey Observatory, 3, 53
- Stephenson, C. B. 1996, VizieR Online Data Catalog, 3156, 0
- Tabur, V., Bedding, T. R., Kiss, L. L., et al. 2010, MNRAS, 409, 777
- van Belle, G. T., Lane, B. F., Thompson, R. R., et al. 1999, AJ, 117, 521
- Walkowicz, L. M. & Basri, G. S. 2013, MNRAS, 436, 1883
- Watson, C., Henden, A. A., & Price, A. 2014, VizieR Online Data Catalog, 1, 2027
- Wiśniewski, M., Marquette, J. B., Beaulieu, J. P., et al. 2011, A&A, 530, A8
- Wood, P. R. & Sebo, K. M. 1996, MNRAS, 282, 958
- Worthey, G. & Lee, H.-c. 2011, ApJS, 193, 1
- Woźniak, P. R., McGowan, K. E., & Vestrand, W. T. 2004, ApJ, 610, 1038
- Wray, J. J., Eyer, L., & Paczyński, B. 2004, MNRAS, 349, 1059
- Zacharias, N., Finch, C. T., Girard, T. M., et al. 2013, AJ, 145, 44

Table 2. Stellar parameters of C1.

ID(CoRoT)	ID	RA[deg.]	DEC[deg.]	ST	LC	Type	V	V_0	I	I_0	J	J_0	K	K_0	$T_{eff}(K)$	P(day)	A(mmag)
101112162	UNC	291.6292	1.1659	M0	II	Semi-sinV*	13.90	12.32±0.17	11.84	10.62±0.14	9.94	9.52±0.09	8.81	8.63±0.06	3999±102	2.61, 16.4, 4.44	4.37, 2.85, 2.03
102285797	102285797	92.2382	4.5606	M3	III	Semi-sinV*	12.91	12.08±0.25	-	-	8.49	8.27±0.13	7.21	7.12±0.09	3591±68	19.0, 17.1, 56.1	36.6, 12.7, 12.7
102299158	102299158	92.4169	5.1898	M0	III	Semi-sinV*	12.93	12.32±0.22	10.85	10.24±0.18	9.12	8.96±0.11	7.89	7.82±0.08	3716±76	37.0, 16.8, 25.1	28.7, 11.6, 13.4
102311422	UNC	92.5670	4.4369	M6	III	Semi-sinV*	14.50	13.70±0.26	-	-	7.64	7.42±0.14	6.20	6.11±0.09	3211±47	118, 79.8, 29.9	216, 27.8, 12.3
102335279	UNC	92.8541	5.1593	M4	III	Semi-sinV*	13.15	12.55±0.24	10.20	9.44±0.19	7.87	7.70±0.12	6.53	6.46±0.08	3375±51	104, 26.8, 43.4	339, 20.9, 18.5
102338552	102338552	92.8902	5.0779	M1	III	Semi-sinV*	12.93	12.24±0.24	10.72	10.03±0.19	8.92	8.74±0.12	7.68	7.60±0.08	3674±73	22.4, 32.2, 27.4	24.7, 20.7, 13.1
102349003	102349003	93.0078	4.5821	M1	III	Semi-sinV*	14.25	13.25±0.21	11.92	11.03±0.17	9.95	9.68±0.11	8.63	8.52±0.07	3647±62	23.0, 26.0, 70.1	23.6, 15.4, 17.6
102354589	102354589	93.0736	4.3677	M2	III	Semi-sinV*	14.06	12.88±0.21	11.68	10.67±0.17	9.69	9.38±0.11	8.30	8.16±0.08	3652±63	42.7, 58.3, 41.2	58.9, 26.0, 10.2
102369726	UNC	93.2538	5.1756	M3	II	Semi-sinV*	13.55	12.58±0.22	10.82	9.87±0.18	8.63	8.37±0.11	7.25	7.14±0.08	3487±55	28.9, 45.3, 36.2	151, 24.9, 14.1
102388262	102388262	93.4664	4.8155	M5	III	Semi-sinV*	13.95	12.89±0.24	10.67	9.57±0.19	8.09	7.81±0.12	6.71	6.59±0.08	3344±48	17.5, 20.0, 24.2	94.9, 20.9, 19.1

Table 3. Stellar parameters of C2.

ID(CoRoT)	ID	RA[deg.]	DEC[deg.]	ST	LC	Type	V	V_0	I	I_0	J	J_0	K	K_0	$T_{eff}(K)$	P(day)	A(mmag)
102371380	UNC	93.2726	5.4890	M1	III	Semi-sinV*	13.59	12.57±0.22	12.06	11.26±0.18	10.51	10.24±0.11	9.51	9.39±0.08	4238±143	21.5	126
102573436	UNC	100.1715	0.6706	M1	III	Semi-sinV*	12.67	10.63±0.22	10.87	9.43±0.18	9.13	8.59±0.11	8.04	7.80±0.08	4434±181	3.94	19.4
102596573	UNC	100.3367	0.9047	M1	III	Semi-sinV*	16.00	13.71±0.35	14.11	12.49±0.28	12.31	11.71±0.18	11.28	11.02±0.12	4526±267	59.5	35.5
102638059	UNC	100.5269	-1.3317	M2/M2	III/III	Semi-sinV*	15.92	14.36±0.21	14.09	12.90±0.17	12.49	12.08±0.11	11.52	11.34±0.08	4327±146	28.2	2.15
102630805	UNC	100.5438	-1.1984	M1/K3	III/III	Semi-sinV*	14.45	13.10±0.24	12.87	11.86±0.19	11.33	10.97±0.12	10.39	10.24±0.08	4414±188	24.5	2.81
102691972	UNC	100.8702	-0.4528	M0/K4	III/III	Semi-sinV*	13.25	12.09±0.19	11.65	10.77±0.15	10.18	9.87±0.10	9.12	8.99±0.07	4280±131	90.3	9.25
102718402	102718402	101.0124	-0.8071	M1/M1/K3	III/III/II	Semi-sinV*	15.91	14.37±0.23	14.23	13.10±0.18	12.61	12.20±0.11	11.59	11.41±0.08	4361±178	11.6	1.87
102726142	UNC	101.0598	-1.2476	M2	III	Semi-sinV*	12.61	10.67±0.30	10.75	9.34±0.24	9.01	8.50±0.15	7.79	7.57±0.10	4279±186	14.7	4.07
102739465	UNC	101.1351	1.0326	M1	III	Semi-sinV*	13.38	11.62±0.41	11.59	10.31±0.33	9.91	9.44±0.21	8.79	8.58±0.14	4316±255	2.94	2.92
102748357	102748357	101.1845	-1.6619	M1	III	Semi-sinV*	16.05	13.92±0.17	14.00	12.43±0.13	12.54	11.98±0.08	11.60	11.36±0.05	4606±167	8.18	55.0

Table 4. Stellar parameters of C3.

ID(CoRoT)	ID	RA[deg.]	DEC[deg.]	ST	LC	Type	V	V_0	I	I_0	J	J_0	K	K_0	$T_{eff}(K)$
102659593	IRAS 06401+0057	100.7014	0.9100	M1	III	LPV*	15.35	13.69±0.25	11.91	10.51±0.20	8.98	8.54±0.13	6.73	6.54±0.09	3248±75
102753101	DJM 35	101.2107	0.8374	M1	III	C*	15.73	14.05±0.28	11.59	10.13±0.22	9.25	8.80±0.14	5.72	5.52±0.09	3151±36
102756832	UNC	101.2318	-2.0673	M5	III	LPV?	16.57	14.61±0.22	12.10	10.27±0.17	8.71	8.19±0.11	6.95	6.73±0.07	3189±45
102798403	UNC	101.4759	-2.3579	M2	I	LPV?	13.96	11.68±0.35	11.97	10.29±0.28	10.61	10.00±0.18	9.74	9.48±0.12	4873±318
102862904	UNC	101.9196	-2.4779	M2	III	LPV?	16.85	14.05±0.24	13.69	11.57±0.18	10.89	10.15±0.11	9.18	8.86±0.08	3538±63
102868800	UNC	101.9532	-2.0940	M2	III	LPV?	16.87	13.96±0.22	13.36	11.15±0.17	10.31	9.54±0.11	8.47	8.14±0.07	3417±47
102885433	DJM 47	102.0524	-0.9607	M1	III	C*	14.56	12.94±0.19	10.76	9.35±0.15	7.80	7.37±0.10	5.46	5.28±0.06	3205±45
102921590	UNC	102.2414	-1.5149	M2	III	LPV?	13.58	12.00±0.22	11.47	10.26±0.18	9.50	9.08±0.11	8.18	8.00±0.08	3878±92
102930515	UNC	102.2867	-1.1656	M0	III	LPV?	13.48	11.75±0.19	11.94	10.71±0.15	10.54	10.08±0.10	9.59	9.40±0.07	4752±187
102994604	IRAS 06480-0305	102.6317	-3.1452	M6	III	LPV*	16.04	14.08±0.19	11.44	9.58±0.14	7.97	7.45±0.09	6.26	6.04±0.06	3179±35